In vivo generation of chimeric antigen receptor T cells using optimally retargeted and functionalized lentiviral vectors with reduced immune clearance

Kepler S. Mears[1,2,†], Kyrellos Ibrahim[1,2,†], Peter M. Allen[1,2,†], Jordan M. Chinai[1,2,3,‡], Omar I. Avila.[1,2,‡], Audrey J. Muscato[1,2,‡], Sarah K. Lane-Reticker[1,2], Alexander Rojas[1,2], Nelson H. Knudsen[1,2], Chun-Cheih Chao[1,2] , Kathleen B. Yates[1,2,#,*], Robert T. Manguso[1,2,#,*]

[1]Broad Institute of Massachusetts Institute of Technology and Harvard, Cambridge, MA, USA.

[2]Krantz Family Center for Cancer Research and Department of Medicine, Massachusetts General Hospital, Boston, MA, USA.

[3]Dana-Farber Cancer Institute, Gastrointestinal Cancer Center, Boston, MA, USA.

† These authors contributed equally

‡ These authors contributed equally

# These authors jointly supervised this work

* To whom correspondence should be addressed: yates@broadistitute.org, rmanguso@broadinstitute.org

Abstract

Despite striking efficacy against hematologic malignancies, the cost and complexity of CAR T manufacturing present significant barriers to broader patient access. Beyond manufacturing challenges, *ex vivo* expansion of T cells may be detrimental for their function and persistence. Thus, delivery of CARs to reprogram host cells *in vivo* would represent a significant advance toward “off-the-shelf” therapy but has been limited by low efficiency, low specificity, and immunogenicity of viral vectors. Here we describe the design of pseudotyped lentiviral vectors (LV) with superior functionality and high target specificity. We show that LV pseudotyped with chimeric envelope glycoproteins from dolphin morbillivirus (DMV) can be engineered to selectively infect human T cells and evade neutralizing antibody responses in measles-vaccinated human serum. We further demonstrate that camelid-derived nanobodies are a superior retargeting domain, overcoming limitations inherent to the use of single chain variable fragment antibodies. Using a chimeric DMV-pseudotyped virus targeting the CD7 receptor, we demonstrate efficient and highly specific infection of T cells both *in vitro* and *in vivo*, generating functional CAR T cells and inducing therapeutic efficacy in a preclinical B cell lymphoma model.

Introduction

Efficient and selective genetic reprogramming of host cells *in vivo* is a major goal for cell and gene therapy. Replication-incompetent lentiviral-like particles (LVs) have been extensively developed for genetic and protein delivery applications for both research and therapeutic applications[1–3]. LVs are enveloped vectors and will incorporate any transmembrane proteins from the producer cell on their surface. The tropism of LVs can be modified through pseudotyping: heterologously expressing different viral-derived and engineered proteins that are incorporated into the envelope during production[4–7]. Pseudotyping most commonly employs the vesicular stomatitis virus glycoprotein (VSV-G), which binds to the widely expressed low-density lipoprotein receptor (LDLR), providing broad tropism for many cell types and mammalian species. VSV-G pseudotyped LVs are currently used to generate chimeric antigen receptor (CAR) T cells *ex vivo* to treat hematological cancers. However, VSV-G provides minimal cell type selectivity and has been difficult to engineer for specificity, limiting its *in vivo* utility[8,9].

Specific retargeting of LVs can be achieved through direct engineering of the pseudotype by the addition of a cell-selective targeting domain and has been successfully deployed to selectively transduce lymphocyte subsets[7,8,10–14]. The Measles Virus (MeV) envelope proteins have been demonstrated to be particularly amenable for retargeting LVs to a broad array of targets[15–17]. Measles, and all other paramyxoviruses, utilize a tetrameric hemagglutinin (H) protein for target receptor recognition and a separate trimeric fusion (F) protein to mediate membrane fusion[18,19] (**Figure 1A**). Receptor recognition by the H protein triggers fusion to the target cell membrane through the F protein, a mechanism that bypasses the need for endocytosis of the viral particle that is a requirement for many viral Envs. By fusing a targeting domain to the H protein, the receptor preference can be altered. Residues in MeV-H can be further mutated to abolish binding to its natural receptors (SLAMF1 and NECTIN4), preventing aberrant transduction on non-target cells. The MeV Env has been demonstrated to provide highly selective targeting to many targets including those that are not endocytosed[8,20,21]. Single chain variable fragments (scFvs) derived from antibodies, DARPins, and cytokines have all been successfully implemented as targeting domains (**Figure 1A, middle**)[9,12,22–24]. Fusion of MeV-H to scFvs and DARPins targeting human CD8 or CD4 have been used to transduce T cells *in vitro,* and to generate functional CAR T cells to treat B cell lymphomas in humanized mouse models[10,11].

Engineered MeV pseudotypes for *in vivo* CAR T therapy have been limited by several significant hurdles. First, fusion of scFvs to MeV-H can lead to intermolecular VH-VL pairing and reduced stability, resulting in poor functional titer and requiring screening of several scFv sequences to identify effective targeting domains[25]. Second, patients vaccinated against measles have neutralizing antibodies directed towards MeV-H and MeV-F[26,27]. Here we describe two technical advances to address these challenges: First, we find nanobodies (VHHs) are more successful targeting domains for MeV-H fusions and mediate efficient viral entry. Second, we demonstrate that the ectodomains from the H proteins of related morbilliviruses can be used to create chimeric Env proteins that maintain fusogenic ability, while avoiding humoral immunity, and can be successfully retargeted with VHH to pseudotype LVs. We show that retargeted LVs pseudotyped with a chimeric measles virus/Dolphin Morbillivirus (DMV) Env displaying a anti-hCD7 VHH can evade anti-MeV-H neutralizing antibodies and selectively transduce human T cells *in vitro* and *in vivo* to create CAR T cells. The described methods are an advance towards the generation of efficient and specific off-the-shelf CAR T therapies.

Results

Camelid-derived nanobodies are superior targeting domains for measles-virus pseudotyped lentiviral transduction

With the goal of creating targeted LVs for CAR T therapy, we initially designed MeV-H-scFv fusions targeting lineage-defining cell markers for T cells and other immune cells for proof of concept *in vivo* experiments. We obtained commercially available hybridomas with specificity for T cell lineage receptors (CD4, CD8a and Thy1) and sequenced the immunoglobulin complementarity determining region (CDR) sequences to create scFvs (**Extended Data Table 1**)[28]. scFvs were cloned into expression vectors such that the scFv sequence was fused to the extracellular domain of wild-type MeV-H (**Figure 1A, left**). We generated LVs with a GFP transgene pseudotyped with VSV-G or retargeted MeV-H-scFv fusions and evaluated transduction in unmodified, receptor-negative murine MC38 colon cancer cells, or MC38 cells engineered to overexpress target matched receptors (Thy1.2, CD4, or CD8a). As a positive control for re-targeting, we generated LV pseudotyped with a human CD105-targeted MeV envelope previously described (MeV-H-αhCD105^{scFv}), with a corresponding hCD105 overexpressing MC38 cell line[17]. MeV does not bind mouse NECT4 or Slamf1 naturally, so we did not receptor-inactivate MeV-H enabling us to utilize MC38 cells overexpressing human NECT4 as a positive control. WT MeV pseudotyped LV provided moderate transduction of MC38 cells expressing the native receptor NECTIN4 (**Extended Data Figure 1A**).

All LVs pseudotyped with in-house MeV-H-scFvs demonstrated minimal or no transduction of cognate receptor expressing MC38 cells expressing, while the published MeV-H-hCD105^{scFv} did result in some measurable transduction (**Extended Data Figure 1A**). Most MeV-H-scFvs were able to transduce the native NECTIN4 indicating the engineered envelopes were still fusion competent. We concentrated LVs pseudotyped with our best performing MeV-H-αmThy1.2A^{scFv} which provided a slight increase in transduction of mThy1.2 MC38 cells (**Extended Data Figure 1B**). As overexpression cell lines do not strictly recapitulate the native protein, we attempted transduction of primary mouse splenocytes with endogenous Thy1.2 expression with lentivirus pseudotyped with the MeV-H-αmThy1.2A^{scFv} and did observe specific transduction (**Extended Data Figure 1C**), however the signal was unstable over the subsequent days. Our results suggest that improper receptor expression, and function of the retargeted envelope, do not explain the low transduction rates we observed using MeV-H-scFv retargeted lentivirus.

We hypothesized the poor transduction efficiencies could be due to low surface expression of the MeV-H-scFv in the HEK293T packaging cells as LV pseudotyping relies on abundant surface expression of viral glycoproteins on the packaging cell line for incorporation into virus particles. We transfected HEK293T cells with HA-tagged MeV-H-scFv expression vectors targeting CD4, Thy1, and CD8a, and compared cell surface expression of the fusions to surface expression of WT MeV-H (**Figure 1B**). Surface expression of MeV-H-scFv fusions was consistently lower than MeV-H alone or the previously reported MeV-H-αhCD105^{scFv} (**Figure 1C, Extended Data Figure 2A**)[17]. Moreover, the level of surface expression across HA-tagged MeV-H fusions correlated with transduction rates of hNECT4 MC38 cells (**Extended Data Figure 2B**), suggesting that viral retargeting was impeded by poor surface expression of the engineered envelope proteins.

scFvs are prone to aggregation due to the hydrophobic domains of VH and VL which facilitate their association in natural antibody tertiary structure[29]. However, in the context of an scFv, these regions can facilitate self-aggregation and mispairing[30]. To address whether inherent stability of scFvs impacted surface expression we purified His-tagged soluble scFvs from HEK293 cells. We observed scFvs that exhibited higher functional titer and/or surface expression also produced higher yields by SDS-PAGE gels (**Extended Data Figure 2C**), suggesting that intrinsic properties associated with scFv expression and/or stability may impact their potential as targeting domains. However, while the Thy1.2A^{scFv} produced purified yields comparable to hCD105^{scFv}, the MeV-H-αThy1.2A^{scFv} fusion exhibited low surface expression and functional titer compared to MeV-H-αhCD105^{scFv}, indicating additional factors contribute to impaired MeV-H-scFv expression.

All purified 6His-tagged scFvs bound their cognate targets on engineered MC38s overexpressing cells *in vitro* (**Extended Data Figure 2D**), leading us to conclude the fusion of the scFv to MeV-H was the driver of low transduction rather than the binding ability of an scFv. To determine whether this phenomenon was generalizable, we evaluated a wider selection of scFvs targeting immune lineage markers including CD45, Thy1, CD4, CD8a, and CD8b and compared surface expression to WT MeV-H (**Figure 1C**, grey bars; **Extended Data Table 1**). Across all scFv sequences tested, we were unable to obtain surface expression comparable to WT MeV-H or the hCD105 scFv fusion (**Figure 1B**, left column; **Figure 1C**, gray bars). Since MeV-H assembles into tetrameric complexes (**Figure 1A**)[18] and the hydrophobic regions of the heavy and light antibody chains within scFvs are prone to aggregation, we hypothesized that the close proximity of multiple scFvs was enhancing aggregation and reducing surface expression (**Extended Data Figure 2E**)[30,31]. As it has been reported that the success of retargeted LVs is highly dependent on the scFv used[25], we sought alternative targeting domains.

Camelid-derived single-domain antibodies (nanobodies or VHHs) are smaller and more soluble than scFvs as they lack a light chain and consequently also lack the hydrophobic domains required for heavy and light chain assembly in human and murine antibodies (**Figure 1D**). We identified published VHHs targeting murine and human immune lineage markers (**Extended Data Table 1**) and cloned a subset into HA-tagged MeV-H expression vectors, then evaluated their surface expression in 293T producer cells. We found much higher surface expression of MeV-H-VHH on the producer cell surface compared to MeV-H-scFvs, at levels comparable to wild-type MeV-H for almost all VHH clones surveyed (**Figure 1B**, right column; **Figure 1C**, orange bars; **Extended Data Figure 2F**). LVs pseudotyped with MeV-H-VHH fusions targeting murine MHC class II or CD45 were generated and applied *in vitro* to activated mouse splenocytes. When compared to transduction using VSV-G-pseudotyped LV, the MeV-H-VHH constructs drove comparable or improved transduction efficiencies with increased target cell selectivity (**Figure 1E).** We then generated similar LVs targeting human CD4, CD8a, or CD7, and applied them to activated human PBMCs which resulted in similar high selectivity when compared to VSV-G, however less efficient transduction. These data suggest that VHH retargeting domains showed improved surface expression and functional titer over scFvs for MeV-H pseudotyped LV.

Recently, several methods of LV targeting have exploited a receptor blind vesicular stomatitis virus glycoprotein (VSV-G) that maintains fusogenic function, referred to as dead VSV-G (dVSV-G) for retargeting. When dVSV-G is expressed in combination with a separate surface protein for receptor targeting, specific delivery can be achieved [32–35]. To benchmark our method to these approaches, we compared transduction of activated primary human T cells with LV

161 pseudotyped with MeV-H-VHH targeting CD7 or LV pseudotyped with dVSV-G and the
162 costimulatory pair of a membrane-bound scFv targeting CD3 and human CD80, and observed
163 similar efficiencies (**Figure 1F**)[33].
164 However, the use of dVSV-G may suffer from a decrease in specificity due to the
165 requirement of low pH via endocytosis to trigger membrane fusion[36], as non-specific interactions
166 can result in endocytosis. Viral targeting using pH dependent Env has been reported to promote
167 such off-target activity[37]. An endocytosis requirement also limits the potential receptors used for
168 targeting. *In vitro* transduction of MC38 cells with LVs pseudotyped with dVSV-G demonstrated
169 that dead VSV-G still drove detectable transduction activity (**Extended Data Figure 3A-B**),
170 suggesting that targeted delivery strategies relying on dVSV-G pseudotyping maintain a risk of
171 off-target transduction. For *in vivo* therapeutic applications, the MeV-H method represents a
172 superior method for true selectivity and VHH a superior targeting domain [8,38].

173 Alternative morbillivirus envelope pseudotyping enables evasion of measles-directed 174 antibodies

175 Broad measles vaccination rates represent a significant potential obstacle to LV
176 retargeting with MeV-H-VHH pseudotyping, as antibodies directed against MeV envelope proteins
177 can neutralize infection, including transduction of MeV pseudotyped LVs [39–41]. We collected sera
178 from a cohort of 21 patients, aged 12 to 75 (median age of 52), that had balanced representation
179 of males and females (**Extended Data Table 2**) and quantified the measles-specific IgG titers of
180 donor samples by ELISA. As expected, the majority were seropositive aside from a single donor,
181 confirming the broad presence of measles targeted antibodies (**Figure 2A**). A subset of donors
182 representing high, medium and low titer was selected for further analysis (**Figure 2A**, colored
183 bars). We developed a serum binding assay to measure serum immunoglobulin (IgG) binding to
184 HEK293T cells expressing HA-tagged MeV-H and -F envelope proteins. HEK293T cells
185 expressing HA-tagged MeV-H or MeV-F were incubated with heat-denatured patient serum
186 before staining with anti-HA and anti-IgG antibodies and analyzing by flow cytometry (**Figure 2B**).
187 Unsurprisingly serum-derived measles-directed antibodies bound surface-expressed MeV
188 envelope glycoproteins in a serum dose- and anti-measles antibody titer- dependent manner
189 (**Figure 2C**), potentially inhibiting the function of the envelope proteins.
190 The mechanism for receptor recognition and envelope fusion is conserved among all
191 morbilliviruses (MoV) and the greater paramyxovirus family[20]. However the surface glycoproteins
192 have low overall sequence similarity, particularly in their extracellular domains, while still
193 maintaining structural homology from AlphaFold3 predictions (**Figure 2D, Extended Data Figure**
194 **4A-B**)[20,42]. Measles-neutralizing antibodies primarily target the extracellular domains of H and F
195 proteins, as such we hypothesized that alternative MoV glycoproteins could be similarly
196 engineered for re-targeting but evade neutralization from preexisting immunity against MeV[43–45],
197 as has been accomplished with Nipah Virus for LVs[46] and CDV for oncolytic virus therapy[27], and
198 modified for MeV [41]. We expressed HA-tagged retargeted hemagglutinin proteins from several
199 morbillivirus species and evaluated surface expression on HEK293T cells compared to a well-
200 expressed MeV-H-αmMHCII^{VHH}. Each retargeted MoV-H fusion protein was successfully
201 expressed on the surface of HEK293T producer cells at levels comparable to MeV-H, except for
202 Phocine mobillivirus (PDV)-H **(Figure 2E, Extended Data Figure 4C**). We attempted to measure
203 wild-type unmodified PDV-H surface expression but were unable to detect any in HEK293T cells

204 (data not shown). In a serum binding assay we observed higher binding of measles-directed
205 antibodies to H proteins of Rinderpest (RPV) and Small ruminant virus (RMV), and reduced
206 binding to the less homologous Canine distemper virus (CDV)- and Dolphin morbillivirus (DMV)-
207 H proteins (**Figure 2F**). As prior work has demonstrated that measles neutralizing antibodies
208 primarily target MeV-H[43–45], we focused our efforts on optimizing CDV and DMV glycoproteins for
209 further engineering and in vivo CAR delivery.
210 DMV-F exhibited high levels of surface expression on HEK293T cells while CDV-F was
211 barely detectable (**Figure 2E**, right). Given the large reduction in anti-measles antibody binding
212 to CDV-H, we attempted to optimize CDV-F expression. We replaced the unusually long signal
213 peptide of CDV-F with shorter alternative signal peptides[47,48] and tested previously reported
214 truncations[49], but were unable to drive higher CDV-F expression (**Extended Data Figure 5A**).
215 DMV-H also exhibited resistance to measles-directed antibody binding and both DMV-H and
216 DMV-F were well expressed in HEK293T, thus we opted to focus on DMV for LV pseudotyping
217 and VHH retargeting. Previous studies found that functional pseudotyping of LVs with MoV
218 required truncation of the cytoplasmic tail of MoV-F[15,50]. We designed DMV-H fused to a VHH
219 targeting mouse MHC-II and co-expressed the construct with full-length or truncated DMV-F to
220 generate LV and compare transduction of target cells to MeV-H-VHH. While we detected low
221 transduction of MHCII+ A20 leukemia cells with DMV-pseudotyped LV, the functional titer was
222 much lower than that of MeV pseudotypes and further engineering would be required to enhance
223 transduction efficiency (**Figure 2G, Extended Data Figure 5B**).

224 Chimerized DMV/MeV glycoproteins improve functional titer while maintaining immune 225 evasion

226 The structural similarities between MoV glycoproteins have been leveraged to create
227 functionally chimeric H hybrid proteins swapping the domains between MoV[51]. MoV-H proteins
228 play a role in triggering membrane fusion through interactions with MoV-F, In addition to receptor
229 recognition. Regions in the globular head (aa244-250) and in the stalk (aa84-105) of MeV-H have
230 been shown to interact with MeV-F[52]. Functional hybrids of MeV/CDV glycoproteins have been
231 created that preserve the key interactions between species-matched H and F domains have been
232 successfully pseudotyped, in addition to resisting neutralization by measles-immune serum[51]. We
233 hypothesized a similar strategy could produce chimeric proteins that preserve the functional MeV-
234 H core while decreasing immune recognition with the ectodomains of DMV or CDV (**Figure 3A**).
235 Chimeric MeV/DMV-H and MeV/CDV-H were generated with the HA tagged αMHCII^{VHH} and were
236 well expressed on the surface of producer cells (**Extended Data Figure 6A)**. Furthermore, both
237 H protein chimeras produced affected pseudotyped LVs with MeV-F, that demonstrated
238 comparable if not superior functional titer when applied to A20 cells (**Figure 3B**).
239 Neutralizing responses to measles are predominantly directed toward MeV-H with some
240 reports suggesting MeV-F is also targeted[44,45]. We detected some serum antibody binding to most
241 MoV-Fs with the functional titer of wild-type DMV-pseudotyped lentivirus being too low to
242 accurately test neutralization (**Figure 2G**). We reasoned that by generating chimeric DMV/MeV-
243 F proteins, we could further reduce potential neutralization while maintaining high viral titers
244 (**Figure 3C**). MoV-F proteins are type I transmembrane proteins so to replace the ectodomain
245 requires substitution of the N terminus and signal peptide. We designed and confirmed surface
246 expression of several chimeras DMV and MeV Fusion constructs with increasing contributions of

247 DMV-derived ectodomain (**Figure 3D**). We generated LVs pseudotyped with each chimera
248 construct paired with MeV/DMV-H-αMHCII^{VHH} or MeV-H-αMHCII^{VHH} and assessed transduction
249 of A20 cells. Only the DMV^{311}/MeV-F construct exhibited comparable transduction efficiency of
250 target cells compared to MeV-pseudotyped LV, confirming the chimeric proteins retained critical
251 interactions and fusogenic capacity (**Figure 3E**). Parallel attempts to functionalize chimeric
252 CDV/MeV-F, including the signal peptide modifications and additional rational engineering
253 strategies, failed to generate well-expressed or functional CDV/MeV-F chimeras **(Extended Data**
254 **Figure 6B-C)**.
255 The MeV-DMV-H chimera had a large reduction in serum binding while theDMV^{311}/MeV-
256 F demonstrated no change (**Figure 3F**). However not all antibody responses are neutralizing, so
257 we performed serum neutralization assays (as previously described) with the MeV/DMV-H-
258 αMHCII^{VHH};DMV^{311}/MeV-F-pseudotyped LVs applied to A20 cells and compared to VSV-G-LVs
259 and MeV-αMHCII^{VHH}-LVs (**Figure 3G**). Across serum three donors we observed a significant
260 increase in average transduction of the dual-chimeric approach compared to MeV-αMHCII^{VHH}-LV,
261 and rates comparable to the VSV-G-LV condition (**Figure 3H)**. Despite reported low levels of
262 VSV-G-specific antibodies in humans[53], we observed a dose-dependent decrease in transduction
263 with the VSV-G-LV, suggesting non-specific factors in human serum limit *in vitro* transduction[54]
264 (**Figure 3H**, black). Collectively, this data demonstrates chimerization successfully evaded
265 measles-specific antibody neutralization. With a successful fully chimeric immune resistance and
266 selective re-targeted pseudotyping strategy in hand, we set out to evaluate feasibility of *in vivo*
267 targeting for CAR T generation using this approach.

268 Retargeted LV enables CAR T generation and killing in mixed *in vitro* cultures

269 *In vivo* CAR T cell generation poses a challenge as resting T cells are extremely resistant
270 to lentiviral transduction[55–57]. During conventional *ex vivo* CAR T cell manufacturing, T cells are
271 activated and expanded *in vitro*, which increases expression of LDLR, the receptor for VSV-G,
272 increasing the transducability of the cells[58,59]. T cell activation also induces effector differentiation
273 and increases cytotoxic functions, enhancing the therapeutic potential of the CAR T cells when
274 reintroduced to the patient[60]. Activation of T cells in both research and clinical contexts is typically
275 accomplished with reagents derived from antibodies targeting CD3 and CD28 to deliver TCR
276 stimulation and costimulation, respectively, as well as supplemental cytokines[61]. For *in vivo*
277 generation of CAR T we set out to incorporate co-activation signals to drive T cell activation and
278 expansion in our re-targeted LVs. We engineered producer HEK293T cells to express both a
279 membrane-tethered scFv targeting CD3 (αCD3) and human CD80, the natural ligand for the T
280 cell costimulatory receptor CD28. These cell surface molecules would then be incorporated into
281 virions, as has been previously described, and activate target T cells[33]. As CD19 CAR T products
282 composed of mixed CD8+ and CD4+ cells are associated with superior and more durable
283 responses[38,62], we elected to use a pan T cell targeting construct MeV/DMV-H-αCD7^{VHH} for CAR
284 delivery and included a GFP reporter.
285 We first tested the activation of primary T cells co-cultured with unmodified or αCD3/CD80
286 HEK293T cells in vitro, and observed significant upregulation of T cell activation markers CD25
287 and CD69 in the αCD3/CD80 condition (**Extended Data Figure 7**). We generated CAR-GFP LV
288 in unmodified HEK293T or αCD3/CD80 HEK293T cell lines, with either VSV-G and MeV/DMV-H-
289 αCD7^{VHH} pseudotypes and tested their transduction and activation of primary T cells *in vitro*

290 (**Figure 4A**). We tested both unstimulated human primary T cells and pre-stimmulated T cells
291 using standard αCD3/αCD28 bead-based activation, and measured activation by expression of
292 CD69 and transduction by GFP fluorescence. As expected, T cells preactivated with beads
293 showed high levels of activation markers and GFP expression regardless of packaging cell line
294 and pseudotype, though LV carrying αCD3/CD80 drove further increases in activation and GFP+
295 cells (**Figure 4B**, top). Transduction of non-activated T cells with αCD3/CD80 HEK293 produced
296 LVs induced a marked increase in CD69 and GFP expression compared to standard HEK293
297 (**Figure 4B**, bottom). These data support that LVs enhanced with αCD3/CD80 can successfully
298 drive activation of target T cells and enhance transduction efficiency.
299 To confirm that αCD3/CD80 enhancement did not impact the specificity of the chimeric
300 retargeting approach we used MeV/DMV-H-αCD7^{VHH} LVs to transduce a mixed population of
301 wildtype (CD7+) and CRISPR knock out (CD7-) Jurkat T cells. MeV/DMV-H-αCD7^{VHH} LV only
302 transduced CD7+ cells, with minimal GFP signal detected in Jurkats lacking expression of CD7
303 while VSV-G-LVs transduced both populations equally (**Figure 4C**). In an *in vitro* co-culture assay
304 we mixed unstimulated human primary T cells with CD19+ NALM6 B cell lymphoma cells at
305 varying effector to target ratios (**Figure 4D**), then we added αCD3/CD80 enhanced LVs
306 pseudotyped with VSV-G or MeV/DMV-H-αCD7^{VHH} and monitored T cell activation, CAR+, and
307 tumor killing by flow cytometry. By Day 3 a significant proportion of the CD19+ NALM6 cancer
308 cells were CAR+ in the VSV-G-LV condition, while the MeV/DMV-H-αCD7^{VHH} LV only transduced
309 T cells (**Figure 4E**). This effect grew more pronounced by day 6, which was also marked by a
310 relative expansion of CAR+ T cells and a reduction in total NALM6 cancer cells in the MeV/DMV-
311 H-αCD7^{VHH} condition (**Figure 4E**). Indeed, as the ratio of effector to target cells increased in
312 MeV/DMV-H-αCD7^{VHH} wells, we observed a significant reduction in total recovered NALM6 cells
313 at the earlier time point, and all conditions eliminated target CD19+ cells by day 6 (**Figure 4F**). In
314 the VSV-G-LV condition by contrast only CAR+ cancer cells were detected in co-culture, and we
315 were unable to detect CAR T generation or cancer-directed cytotoxicity. Surface enhanced and
316 retargeted LV can specifically and successfully generate CAR T cells in a heterogeneous context
317 without the need for additional T cell stimulation.

318 ## *In Vivo* administration of retargeted LV generates effective CAR T response

319 With successful *in vitro* experiments we moved on to *in vivo* models using an LV composed
320 of MeV/DMV-H-αCD7^{VHH}, DMV^{311}/MeV-F, and αCD3/CD80, now referred to as Targeted and
321 Stimulatory Engineered Lentivirus (TaSEL) (**Figure 4A**, bottom right). We used a xenograft
322 mouse model to evaluate the capacity of TaSEL vectors to generate human CAR T cells *in vivo*
323 and compared anti-tumor efficacy to conventional *ex vivo* generated CAR T cells. Luciferase-
324 expressing NAML6 B cell leukemia cells were injected into immunodeficient NOD.Cg-
325 *Prkdc*^{scid}*Il2rg*^{tm1Wjl}/SzJ (NSG) mice at day -8 to establish B-ALL tumors. On day -1, a subset of
326 mice then received intravenous (i.v.) injections of human T cells, of which one cohort also received
327 a single injection of TaSEL delivering αCD19 CAR-GFP and the other received no virus. As a
328 control for the expected efficacy of CAR T cell therapy in this model, we included a group of tumor-
329 bearing mice treated with a dose of conventional αCD19 CAR-GFP T cells made ex vivo (**Figure**
330 **5A)**. Throughout the experiment, mice were imaged twice weekly to monitor tumor burden, and
331 peripheral blood was collected weekly via submandibular bleeds to assess CAR T production.

At day 6 post injection the transferred human T cells had engrafted into mice and TaSEL had successfully transduced target T cells to generate CAR+ T cells *in vivo* at frequencies comparable to that of conventional CAR T cell transfer (**Figure 5B**). Additionally, no GFP fluorescence was detected in off-target cell populations by flow, indicating highly selective transduction by TaSEL (**Figure 5C).** To understand the functionality of the CAR T response, we also monitored tumor burden with non-invasive luciferase imaging over time and observed that untreated animals (NALM6 only, T cells only) rapidly succumbed to disease (**Figure 5D-E**). Mice that had received conventional CAR T cells showed modest control and slowing of tumor growth, although none survived beyond 30 days. In the cohort of mice that received T cells and a single dose of TaSEL, two of three mice showed striking and prolonged control of tumor growth and survived long enough that they began showing signs of xenographic graft-versus-host disease (x-GVHD), a common limiting factor in humanized mouse models (**Figure 5D-E**).

We analyzed tissue collected in sacrificed animals for evidence of on- and off-target infection events. Flow cytometry of bone marrow and spleen cells revealed comparable engrafted GFP+ CAR T cell frequencies at endpoint in animals that received either conventional CAR T or *in vivo* administration of TaSEL (**Figure 5F**). Analysis of non-T cell populations (CD3-) in collected blood at endpoint failed to detect off-target transduction in TaSEL-treated mice (**Extended Data Table 3**). CAR-GFP signal was also undetected in off-target cells in the bone marrow or spleen, corroborating our earlier findings in peripheral blood (**Figure 5F**). To further interrogate off-target effects we performed multiplexed immunofluorescence analysis of liver tissue sections to determine whether LV-delivered GFP could be detected in cells other than T cells (αCD3) or Kupffer cells/macrophages (αF4/80), which are known to sequester lentiviral particles in the liver[63,64](**Figure 5G, Extended Data Figure 8**). The GFP+(CAR+) cells identified in these sections were over 99.7% CD3-positive. Across multiple broad tissue sections, no GFP-positive hepatocytes were observed. Rare off-target (CD3-negative) GFP-positive cells were identified at a frequency less than 1/6,700th of that observed within the CD3-positive T cell compartment. These events occurred at such a low frequency that we cannot exclude them as being attributed to fluorescent staining artifacts which are prone to occur in large-tissue multiplex immunofluorescence studies such as this. Thus, *in vivo* delivery of TaSEL can selectively and efficiently generate CAR T with comparable or improved anti-tumor function, relative to conventional manufactured CAR T.

Discussion

Here we demonstrate that TaSEL is a significant advance for *in vivo* CAR T generation that drives efficient and specific cell type transduction and evades broad vaccine-induced immunity and neutralization. To optimize this system for the *in vivo* delivery of chimeric antigen receptors to T cells, we made two major advances: First, we show that the use of camelid-derived heavy chain-only (VHH) antibodies dramatically improves the function of morbillivirus envelope glycoprotein pseudotyping as a strategy for redirecting virus specificity. Second, we generate a chimeric envelope where the extracellular region is derived from dolphin morbillivirus (DMV), which has low amino acid identity with measles virus and substantially evades neutralization from anti-measles antibodies. We further functionalized the retargeted viral particles by incorporating αCD3 and CD80 to activate T cells upon viral encounter to ensure T cells are competent for transduction. These strategies combined enable the selective and efficient delivery of CARs to T

375 cells in an in vivo model, which shows efficacy that is at least comparable to conventional *ex vivo*
376 generated CAR T cells.
377 Lentivirus can be pseudotyped with viral envelope proteins from several families of
378 viruses[4–6,32], and receptor engineering to accomplish cell type-selective retargeting has been
379 demonstrated using envelope glycoproteins from several viruses including Sindbis virus envelope
380 [65–68] and a receptor binding mutated "blind" version of VSV-G[33–35]. However, these exhibit
381 mediocre specificity, likely because membrane fusion requires a pH-dependent trigger from
382 endocytosis[36], which can also result from nonspecific interactions with the host cells, independent
383 of receptor binding[37]. The technologies that have proven to be the most selective are those that
384 employ envelope glycoproteins from the paramyxovirus family, including Nipah virus (NiV) and
385 measles virus[37,46]. Paramyxovirus envelope glycoproteins are multiprotein complexes where the
386 receptor recognition performed the tetrametic H protein, and fusion by the trimeric F protein.
387 Fusion of the envelope complex is triggered by receptor recognition at the cell surface, and is
388 independent of pH or endocytosis[20]. This is an optimal mechanism for receptor retargeting as it
389 eliminates unwanted off-target transduction from the inevitable envelope-independent
390 endocytosis of viral particles[37].
391 While the envelopes of MeV and NiV are amenable to engineering both viruses are human
392 pathogens. Immunity to MeV is widespread in the human population due to worldwide vaccination
393 efforts. Neutralizing antibodies induced by vaccination have been found directed against the
394 envelope H protein and possibly against the F protein of measles[43,69]. While NiV infection is
395 currently rare and immunity in humans not widespread, NiV has a documented history of
396 outbreaks[70]. NiV infection is life-threatening and the World Health Organization has identified
397 Nipah virus as a potential cause of future epidemics and vaccine development efforts are
398 underway[70,71], which would preclude the use of Nipah virus envelope for therapeutic lentiviral
399 engineering.
400 In this work, we have demonstrated that chimeric envelope proteins between different
401 morbillivirus' can pseudotype lentiviral particles and be engineered for cell specific transduction.
402 These viruses are not known to infect humans so future widespread immunity against them is
403 unlikely. Their envelope glycoproteins share significant structural homology with measles virus
404 but have low amino acid identity, and thus the ability for anti-measles antibodies to neutralize
405 transduction via these envelopes is limited. We show here that even in donors with a high anti-
406 measles antibody titer, binding of s chimeric MeV/DMV pseudotyped lentivirus is reduced at least
407 100-fold and neutralization of transduction is equivalent to a VSV-G control. As the conserved
408 epitopes for anti-measles neutralizing antibody binding have been well-studied[69], future work to
409 alter amino acids in these key areas could even further reduce antibody binding. Thus, our method
410 of using dolphin morbillivirus envelope enables specific and neutralization-resistant lentiviral
411 pseudotyping that is not threatened by future public health efforts.
412 The use of camelid-derived single-domain antibodies as the targeting domain is a key
413 advance that enables the high efficiency we observe with TaSEL. Previous work has mainly
414 implemented single chain variable fragment (scFv) antibodies to redirect measles or NiV
415 pseudotyped lentiviral vectors. While scFvs have produced successful re-targeted LVs,
416 optimization is often required with testing many potential scFvs, suggesting that scFvs are
417 generally inefficient for re-targeting[8,25]. We hypothesize that the mechanism for inefficiency is self-
418 aggregation and mispairing via the hydrophobic regions that natively facilitate Vh and Vl binding[30].

419 The intrinsic tendency for self-aggregation of scFvs is well documented [72] and could be
420 exacerbated by the tetrameric H protein complex on the surface leading to poor stability[18]. We
421 observed universally low expression of our designed MeV-H-scFv fusion, supporting the potential
422 aggregation. Other binding domains such as DARPins have been used[24], although no systematic
423 effort has been reported and the success rate for DARPins is unclear. Furthermore DARPins are
424 used infrequently and require screening large display libraries, limiting potential candidates. VHHs
425 on the other hand are increasingly popular and as such many more binders are available. Beyond
426 this, the ability to immunize camelids or the recently developed nanomouse against any target of
427 interest makes the technology more accessible [73].
428 Finally, we demonstrate that our DMV-H protein retargeting system can be combined with
429 lentiviral surface engineering to functionalize viral particles. By engineering viral packaging cells
430 to overexpress an αCD3 scFv and CD80, these molecules can be incorporated into viral particles
431 to enable activation of T cells on contact[33]. Efficient LV transduction of T cells requires T cell
432 activation and proliferation, likely due to retroviral transduction generally being inefficient in non-
433 dividing cells and downregulation of viral restriction factors[74,75]. The majority of circulating T cells
434 in human blood and secondary lymphoid organs have either an effector memory (EM) or central
435 memory (CM) phenotype and are not activated and rapidly proliferating. The inability to efficiently
436 transduce these populations would severely restrict the "accessible" population of T cells in a
437 patient, potentially limiting the efficiency of the product. Additionally, recent evidence suggests
438 that CAR T cells generated from CM T cells have superior efficacy and persistence[76], thus
439 transducing these populations of T cells *in vivo* would be a priority for an off-the-shelf CAR T cell
440 product. Surface functionalization is a prime method for further engineering of LVs.
441 TaSEL provides a significant advantage compared to other current methods of LV re-
442 targeting for *in vivo* use. There are a few limitations of TaSEL, namely in production and further
443 immune reduction. Generally, the MoV based pseudotyping methods result in lower functional
444 titers than VSV-G. The low titers require a large amount of LV to be produced for *in vivo*
445 experiments and they are difficult to concentrate. Optimizations for production and increases in
446 functional titer would be beneficial to creating an off-the-shelf therapy. For reduced immune
447 clearance we focused on DMV for chimerization, however CDV likely provides a further
448 advantage. While we were unable to generate a usable CDV-F construct, the potential for a further
449 reduction in avoidance on neutralizing antibodies is possible. Importantly, we still demonstrate a
450 significant reduction *in vitro* where neutralization is easy to observe, the *in vivo* context may not
451 require as significant reduction to achieve measurable effects.
452 In summary, our TaSEL technology overcomes a series of unique challenges for *in vivo* T
453 cell-focused gene therapy and may represent a path forward to generate off-the-shelf T cell
454 therapeutics for patients. The system could be used for the delivery of any therapeutic payload
455 that can be packaged into a lentiviral vector and applied to any therapeutic area where engineered
456 T cells are currently being evaluated, including hematologic malignancy, solid tumor malignancy,
457 and autoimmune disease. Given the high unmet need in these therapeutic areas and the ongoing
458 challenges of manufacturing engineered autologous T cell products for all patients who could
459 benefit from them, off-the-shelf technologies such as TaSEL should be a major focus for the
460 biotechnology industry.

Acknowledgements

We thank Branka Horvat and the Measles Virus Biobank for the generous gift of the CL55 and Y503 antibodies, INSERM, France, Measles virus Biobank https://ciri.ens-lyon.fr/teams/IbIV/measles-biobank. We thank Nathan Pirete and the Broad Institute Flow Cytometry Core for training and assistance in flow cytometry experiments and the Broad Institute vivarium staff for the assistance with mouse studies. We would like to thank Professor Fritz Melcher from the German Rheumatology Research Center Leibniz-Institute for providing the FGK4.5 hybridoma, Dr. Hasaya Akiba for providing the RMT3-23 hybridoma, and Dr. Yoji Murata for providing the MY-1 and Miap301 hybridomas.

Author information

These authors contributed equally: Kepler S. Mears, Kyrellos Ibrahim, and Peter M. Allen
These authors contributed equally: Jordan M. Chinai, Omar I. Avila and Audrey J. Muscato

Corresponding author

Correspondence to Robert T. Manguso and Kathleen B. Yates.

Ethics Declarations and competing interests

This manuscript was supported in part by funding from Calico Life Sciences, LLC. R.T.M., K.B.Y., K.S.M., K.I., and P.M.A. are authors on a patent related to the technology described in this manuscript. R.T.M. has received speaking or consulting fees from Bristol Myers Squibb, Gilead Sciences, Kumquat Biosciences, Immunai Therapeutics, and BioNTech and has equity ownership in OncoRev, LLC and Jumble Therapeutics.

Author contributions

Conceptualization, K.S.M., K.B.Y., and R.T.M.; formal analysis, K.S.M., P.M.A, K.I., J.M.C., O.I.A., A.J.M, S.K.L-R., A.R. and C.C.; investigation, K.S.M., P.M.A, K.I., J.M.C., O.I.A., A.J.M, S.K.L-R., A.R., N.H.K. and C.C.; resources, K.S.M., P.M.A, K.I., J.M.C., O.I.A., A.J.M, S.K.L-R., A.R., N.H.K. and C.C.; writing – original draft, K.S.M., P.M.A, K.I., J.M.C., K.B.Y., and R.T.M.; writing – review and editing, K.S.M., P.M.A, K.I., K.B.Y., J.M.C., and R.T.M.; visualization K.S.M., P.M.A, K.I., J.M.C.; supervision, , K.S.M., K.B.Y., and R.T.M.

Figure 1: Camelid-derived VHH are a superior targeting domain for MeV-based lentiviral particle retargeting

(A) The hemagglutinin protein of MeV governs target recognition to trigger membrane fusion by proximity;, by adding an exogenous targeting domain the envelope can be re-targeted. (B) Surface expression flow cytometry staining for the MeV-H protein with scFvs and VHHs targeting a variety of relevant murine targets compared to the WT MeV-H protein. (C) MFI ratio of MeV-H-TD vs wt MeV-H for a selection of screened scFvs and VHH. (D) Human antibodies are larger than those from camelids, which lack the light chain and consist of a single heavy domain (VHH). (E) Flow cytometry of primary activated murine splenocytes or human PBMCs transduced with traditional VSVg pseudotyped LV carrying a GFP transgene or VHH re-targeted MeV across several targets. (F) Comparison of anti hCD7 MeV-H-VHH targeted LVs (top) to dVSVG pseudotyped LV with a CD3/28 targeting moiety (bottom).

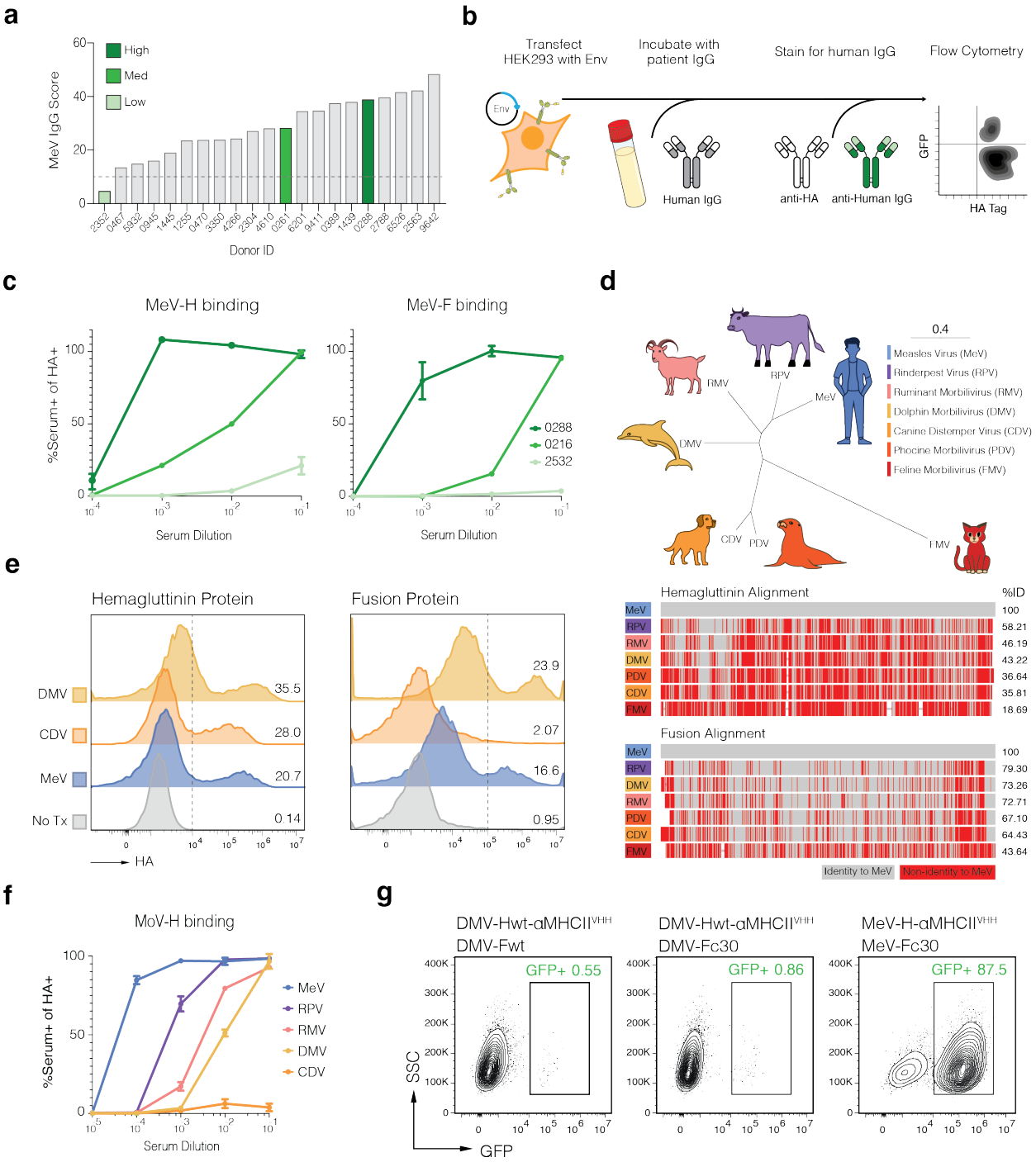
a
MeV IgG Score
High
Med
Low
Donor ID
b
Transfect HEK293 with Env
Incubate with patient IgG
Stain for human IgG
Flow Cytometry
Env
Human IgG
anti-HA
anti-Human IgG
GFP
HA Tag
c
MeV-H binding
MeV-F binding
%Serum+ of HA+
Serum Dilution
0288
0216
2532
d
0.4
Measles Virus (MeV)
Rinderpest Virus (RPV)
Ruminant Morbilivirus (RMV)
Dolphin Morbilivirus (DMV)
Canine Distemper Virus (CDV)
Phocine Morbilivirus (PDV)
Feline Morbilivirus (FMV)
RMV
RPV
MeV
DMV
CDV
PDV
FMV
Hemagluttinin Alignment
%ID
MeV 100
RPV 58.21
RMV 46.19
DMV 43.22
PDV 36.64
CDV 35.81
FMV 18.69
Fusion Alignment
MeV 100
RPV 79.30
DMV 73.26
RMV 72.71
PDV 67.10
CDV 64.43
FMV 43.64
Identity to MeV
Non-identity to MeV
e
Hemagluttinin Protein
Fusion Protein
DMV 35.5
CDV 28.0
MeV 20.7
No Tx 0.14
23.9
2.07
16.6
0.95
HA
f
MoV-H binding
%Serum+ of HA+
Serum Dilution
MeV
RPV
RMV
DMV
CDV
g
DMV-Hwt-αMHCII VHH
DMV-Fwt
GFP+ 0.55
DMV-Hwt-αMHCII VHH
DMV-Fc30
GFP+ 0.86
MeV-H-αMHCII VHH
MeV-Fc30
GFP+ 87.5
SSC
GFP

500 Figure 2: Pseudotyping with alternative morbillivirus glycoproteins can evade measles-
501 directed antibodies

502 (A) Serum reactivity to measles from a cohort of self-reported MMR patients. A subset of low,
503 medium and high reactivity (color bars) was selected for experiments. (B) Flow cytometry assay
504 to determine MeV envelope binding of patient serum. Envelope expressing producer cells are
505 incubated with patient serum, followed by staining with an anti-human IgG to determine serum Ab
506 binding and an HA antibody to measure envelope expression. (C) Results from the assay in (B)
507 for producer cells expressing MeV-H and MeV-F for the subset of patient samples. (D) Genetic
508 distance for the MoV-H proteins in the morbillivirus family (top). Alignment of MoV envelopes to
509 MeV shows low overall sequence similarity for the H protein. (E) Expression of DMV-αMHCII^{VHH},
510 CDV-αMHCII^{VHH} and MeV-αMHCII^{VHH} envelope proteins in HEK293 producer cells. (F) Serum
511 antibody binding to producer cells expressing a subset of MoV-H cells that demonstrated high
512 surface expression. (G) LVs pseudotyped with MHCII-targeted DMV-H demonstrate minimal
513 transduction. Through truncation of the F protein a slight increase was observed but significantly
514 less than measles.

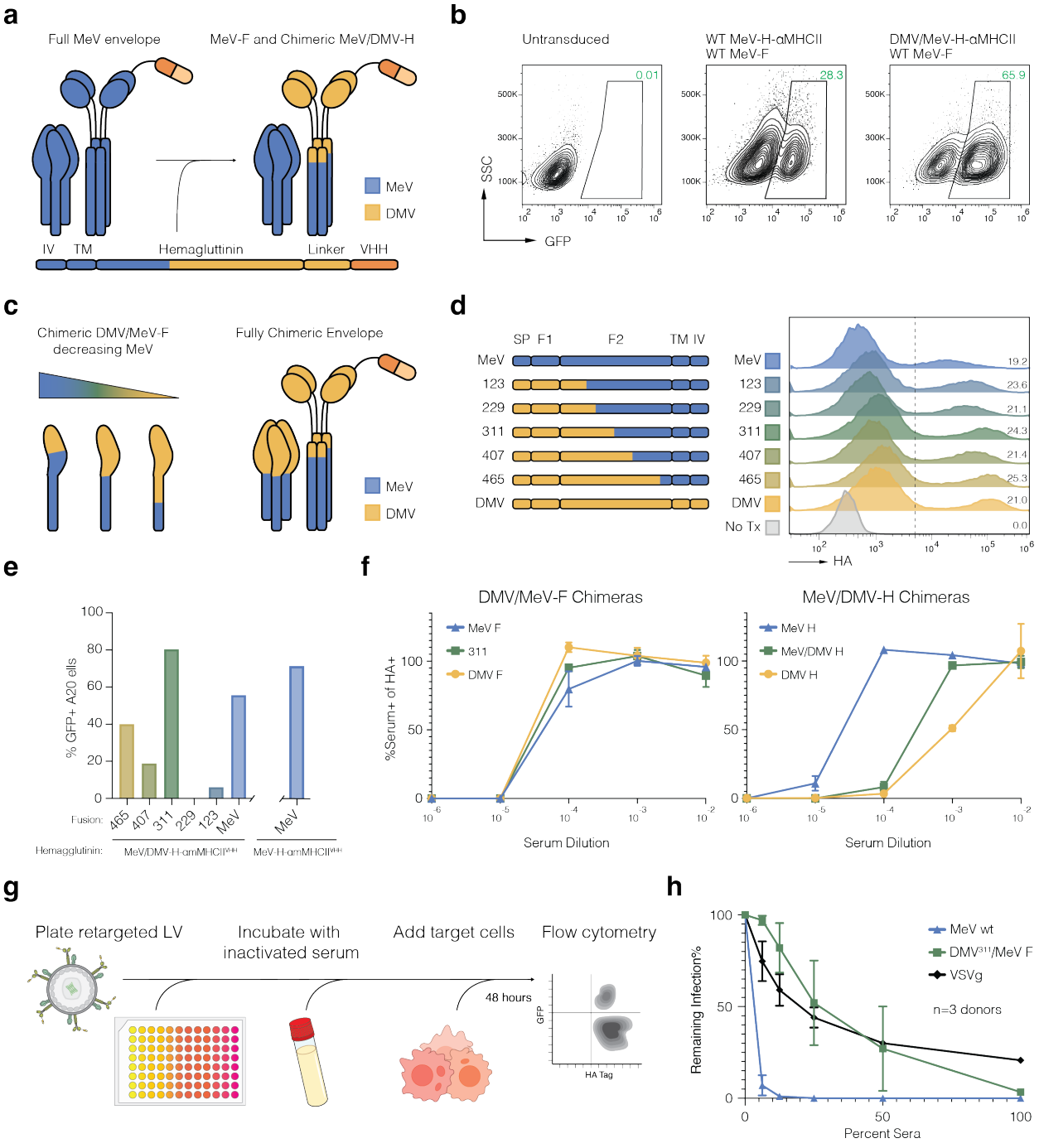
a
Full MeV envelope
MeV-F and Chimeric MeV/DMV-H
MeV
DMV
IV
TM
Hemagluttinin
Linker
VHH
b
Untransduced
WT MeV-H-αMHCII
WT MeV-F
DMV/MeV-H-αMHCII
WT MeV-F
0.01
28.3
65.9
SSC
GFP
c
Chimeric DMV/MeV-F
decreasing MeV
Fully Chimeric Envelope
MeV
DMV
d
SP F1
F2
TM IV
MeV
123
229
311
407
465
DMV
No Tx
19.2
23.6
21.1
24.3
21.4
25.3
21.0
0.0
HA
e
% GFP+ A20 cells
Fusion:
465
407
311
229
123
MeV
MeV
Hemagglutinin:
MeV/DMV-H-αMHCII
MeV-H-αMHCII
f
DMV/MeV-F Chimeras
MeV/DMV-H Chimeras
MeV F
311
DMV F
MeV H
MeV/DMV H
DMV H
%Serum+ of HA+
Serum Dilution
g
Plate retargeted LV
Incubate with
inactivated serum
Add target cells
Flow cytometry
48 hours
GFP
HA Tag
h
Remaining Infection%
MeV wt
DMV311/MeV F
VSVg
n=3 donors
Percent Sera

515 Figure 3: Lentivirus pseudotyped with MeV/DMV chimeric envelope proteins are not
516 neutralized in measles-vaccinated sera

517 (A) Design of chimeric Hemmagluttinin protein. Residues 1-N are MeV while N-End are DMV. (B)
518 Chimeric MeV/DMV-H produces infectious LVs with MeV-F comparable to that of standard MeV-
519 H/F LVs. (C) Design of complementary chimeric fusion proteins. As the MoV-F proteins are type
520 I transmembrane proteins and thus the signal peptide is that of the extravirion MoV. (D) Surface
521 expression of tested chimeric MeV/DMV-F proteins. (E) Transduction of chimeric MeV/DMV-F
522 protein LVs with Chimeric MeV/DMV-H protein (left) and standard MeV-H (right). Chimeric
523 MeV/DMV-H and DMV^{311}/Mev-F produce titers comparable to that of fully MeV pseudotyped LVs.
524 (F) Patient serum binding to chimeric envelope proteins utilizing the assay described in 2B. (G)
525 Flow cytometry assay to determine neutralization of viral particle infectivity. Re-targeted LV is
526 plated in a series of dilutions of patient donor serum. Target cells are then added, and the plate
527 is incubated for 48 hours before analysis by flow cytometry. (H) Quantification of neutralized
528 infection comparing LV pseudotyped with full MeV (MeV-H-$\alpha MHCII^{VHH}$ + MeV-F), chimeric
529 MeV/DMV (MeV/DMV-H-$\alpha MHCII^{VHH}$; DMV^{311}/Mev-F), or VSV-G envelopes (n=3, patient IDs
530 6526, 6201, 9411).

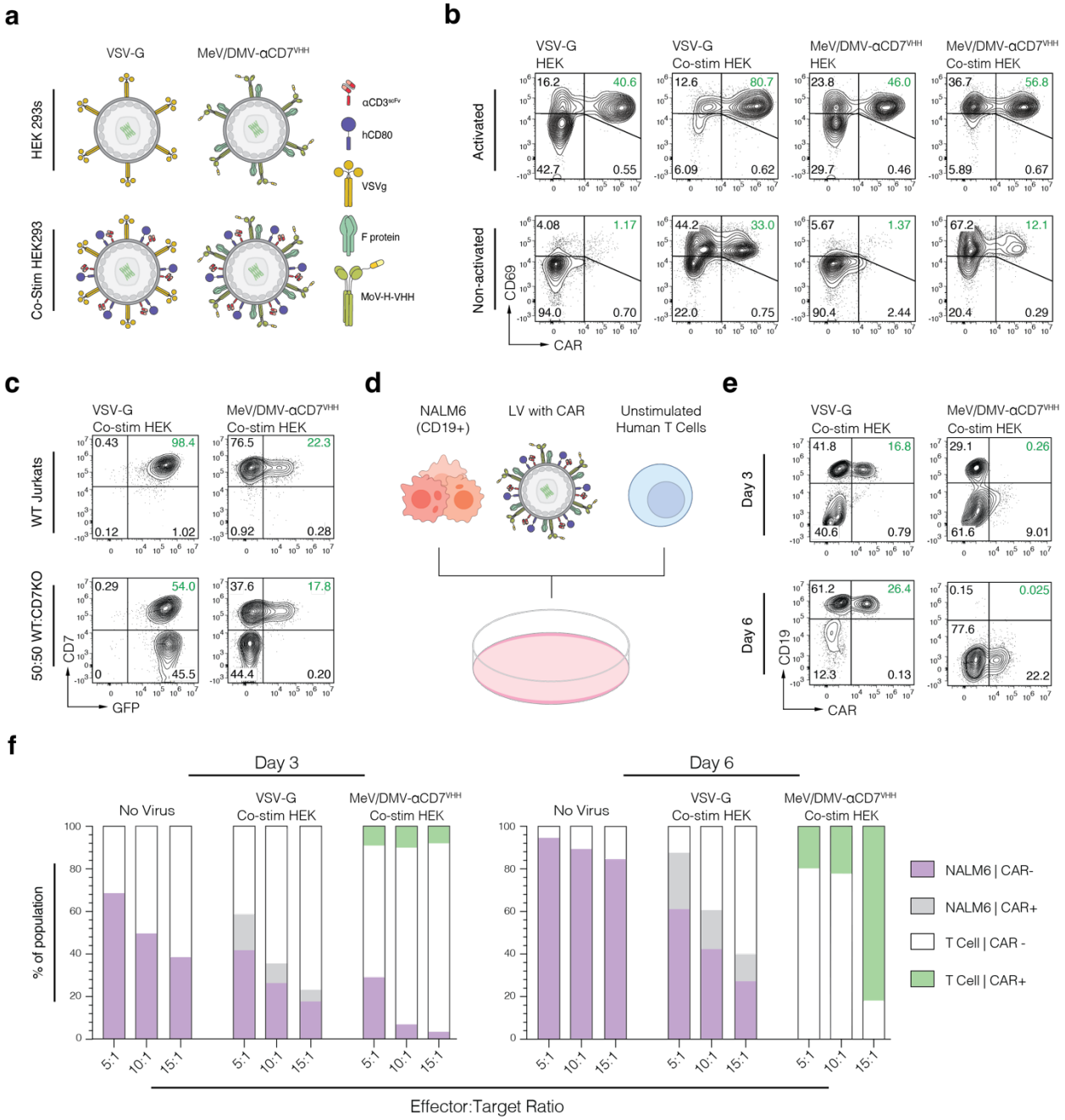
a
VSV-G
MeV/DMV-αCD7VHH
HEK 293s
Co-Stim HEK293
αCD3scFv
hCD80
VSVg
F protein
MoV-H-VHH
b
VSV-G HEK
VSV-G Co-stim HEK
MeV/DMV-αCD7VHH HEK
MeV/DMV-αCD7VHH Co-stim HEK
Activated
Non-activated
CD69
CAR
c
VSV-G Co-stim HEK
MeV/DMV-αCD7VHH Co-stim HEK
WT Jurkats
50:50 WT:CD7KO
CD7
GFP
d
NALM6 (CD19+)
LV with CAR
Unstimulated Human T Cells
e
VSV-G Co-stim HEK
MeV/DMV-αCD7VHH Co-stim HEK
Day 3
Day 6
CD19
CAR
f
Day 3
Day 6
No Virus
VSV-G Co-stim HEK
MeV/DMV-αCD7VHH Co-stim HEK
% of population
NALM6 | CAR-
NALM6 | CAR+
T Cell | CAR -
T Cell | CAR+
5:1
10:1
15:1
Effector:Target Ratio

531 Figure 4: Retargeted and stimulatory LV enables CAR T generation and killing in mixed
532 in vitro cultures

533 (A) Stimulatory functionalization of pseudotyped lentiviral vectors with chimeric MoV targeted
534 envelopes. Co-stim HEK293s have been engineered to express a surface anchored αCD3 scFv
535 and CD80 to enable activation of T cells. (B) Comparison of standard and co-stim functionalized
536 VSV-G and chimeric MeV/DMV αCD7 pseudotypes on pre-activated and unactivated human T
537 cells. Co-stim LVs successfully activate unactivated T cells as measured by CD69 expression
538 and result in greater transduction. (C) Specificity analysis of finalized TaSEL vectors on CD7
539 knock-out Jurkat cells. (D) *In vitro* CAR-T generation and cancer killing assay. Unactivated T cells
540 (effector) and NALM6 (target) cells are mixed at varying ratios with LVs containing a CAR-GFP
541 transgene. (E) Example data from (D) comparing VSVG and TaSEL pseudotypes. (F)
542 Quantification at day 3 and 6 post mix of D with VSV-G and TaSEL pseudotypes at varying
543 effector to target ratios.

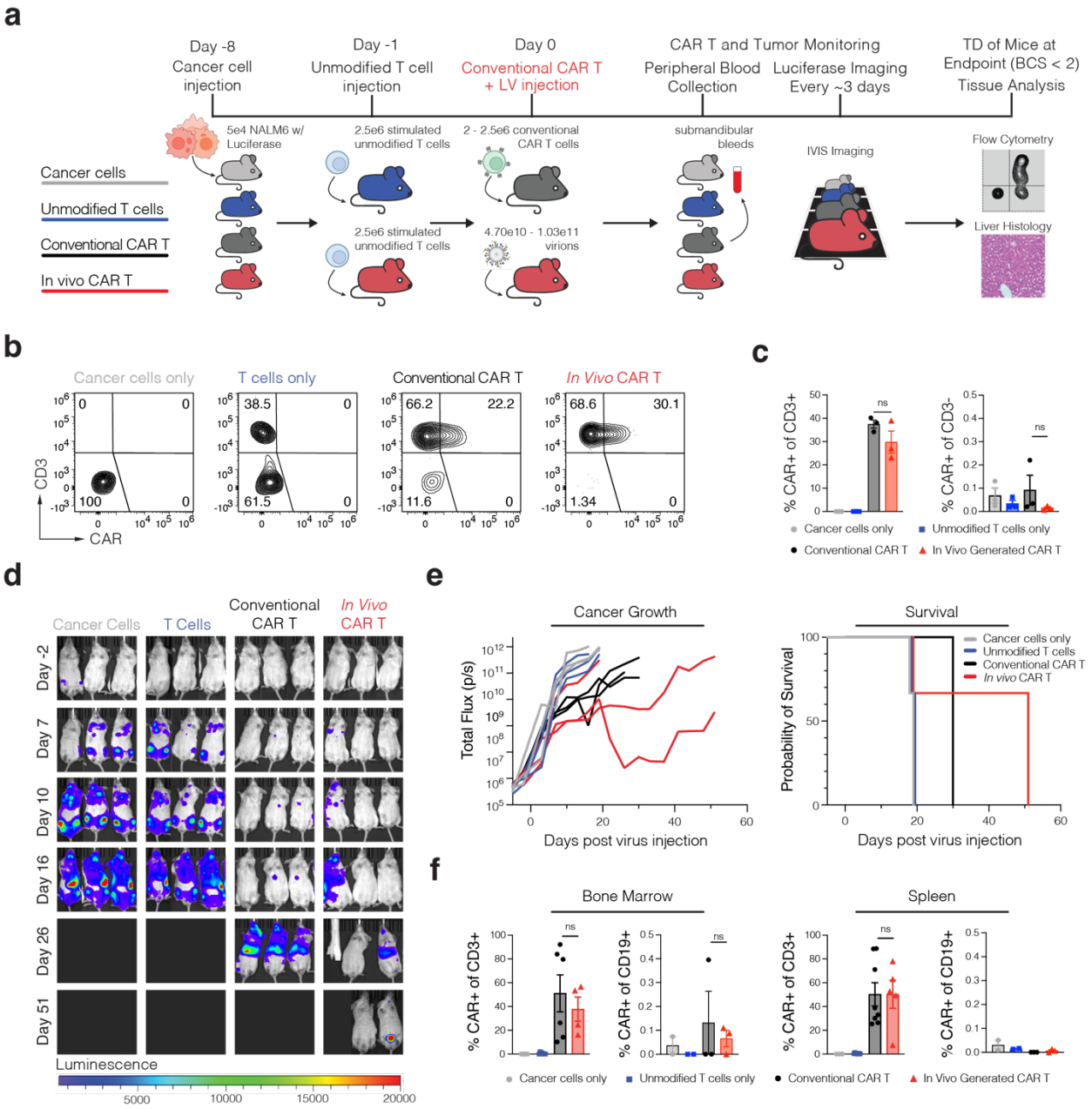
a
Day -8
Cancer cell injection
Day -1
Unmodified T cell injection
Day 0
Conventional CAR T + LV injection
CAR T and Tumor Monitoring
Peripheral Blood Collection
Luciferase Imaging Every ~3 days
TD of Mice at Endpoint (BCS < 2)
Tissue Analysis
Cancer cells
Unmodified T cells
Conventional CAR T
In vivo CAR T
5e4 NALM6 w/ Luciferase
2.5e6 stimulated unmodified T cells
2 - 2.5e6 conventional CAR T cells
2.5e6 stimulated unmodified T cells
4.70e10 - 1.03e11 virions
submandibular bleeds
IVIS Imaging
Flow Cytometry
Liver Histology
b
Cancer cells only
T cells only
Conventional CAR T
In Vivo CAR T
CD3
CAR
38.5
61.5
66.2
22.2
11.6
68.6
30.1
1.34
c
% CAR+ of CD3+
% CAR+ of CD3-
ns
Cancer cells only
Unmodified T cells only
Conventional CAR T
In Vivo Generated CAR T
d
Cancer Cells
T Cells
Conventional CAR T
In Vivo CAR T
Day -2
Day 7
Day 10
Day 16
Day 26
Day 51
Luminescence
5000
10000
15000
20000
e
Cancer Growth
Total Flux (p/s)
Days post virus injection
Survival
Probability of Survival
Cancer cells only
Unmodified T cells
Conventional CAR T
In vivo CAR T
f
Bone Marrow
Spleen
% CAR+ of CD3+
% CAR+ of CD19+
ns
Cancer cells only
Unmodified T cells only
Conventional CAR T
In Vivo Generated CAR T
g
All
GFP (CAR)
Arginase-1
CD3
F4/80
DAPI
h
% CAR+ Cells
T Cells
Hepatocytes
Macrophage
Other Cells

Figure 5: *In vivo* administration of TaSEL generates CAR T cells and controls NALM6 tumors.

544 (A) Experimental scheme for *in vivo* CAR T cell generation and evaluation. Cohorts of mice all
545 received NALM6 leukemia cells expressing luciferase. Control mice either received no T cells or
546 unmodified human pan T cells. Treatment mice received unmodified T cells chased by TaSEL the
547 following day (*In Vivo* CAR) or *ex vivo* generated CAR T cells (Conventional CAR). Analysis
548 consisted of luciferase imaging for tumor quantification, per. (B) CAR T cell content of peripheral
549 blood collected on D6 post virus injection via submandibular bleeds. X-axis is CAR+ (FITC), y-
550 axis is CD3+ (APC) (C) Quantification of CAR+ frequencies in target T cells (CD3+) and off-target
551 cells (CD3-). (D) Representative IVIS imaging at each indicated timepoint following TaSEL
552 administration. Mice not shown were sacrificed according to Body Condition Score guidelines and
553 tissues were collected and analyzed. Bioluminescence overlays represent current tumor burden
554 for a given mouse (E) Quantification of individual mouse tumor burden in radiance
555 (photons/second) over time and probability of survival for each mouse group over time. (F)
556 Quantification of transduction frequencies of cell types of interest in spleen and bone marrow.
557 CD19+ = NALM6 cells, CD3+ = T cells, CAR+ = CAR T cells. Data represents mean ± SEM (all
558 groups n = 3, used one-way ANOVA) (G) Multiplex immunofluorescence staining of liver sections
559 from mice with *In Vivo* CAR. Large tissue sections were stained, imaged, and analyzed. Cell
560 segmentation, and classification was performed followed by assessment of GFP staining
561 intensity. Breakdown of GFP-positive cells (CAR+) within each cell-type is shown. Groups were
562 compared with a Mann-Whitney statistical test.

563 # Methods

564 **Mouse experiments**

565 Immunodeficient NOD.Cg-*Prkdc*^{scid}*Il2rg*^{tm1Wjl}/SzJ (NSG) mice were raised in-house.
566 NALM6 cells, human pan T cells, and TaSEL were all administered via tail vein injections using a
567 rodent restrainer. Tumor cells were prepared by 3 washes in HBSS (Gibco/ThermoFisher
568 14065056) as follows: pellet by centrifugation at 350×g for 5 minutes, decant supernatant, then
569 resuspend at 5e5 - 8e5 cells/mL. Tumor cells were counted with a Countess II (ThermoFisher)
570 and diluted to a final concentration of 5e5 cells/mL HBSS. Mice were administered 100 µL (5e4
571 tumor cells) via tail vein injection 8 days before TaSEL injections. Human pan T cells were
572 similarly prepared with 500×g centrifugation. T cells were counted with a Countess II and verified
573 by hand with a hemacytometer, then diluted to a final concentration of 2.5e7 cells/mL. Mice were
574 administered 100 µL (2.5e6 T cells) via tail vein injection 1 day before TaSEL injections. CAR T
575 cells were generated as described for *In vitro CAR T cell activation and killing assay* and CAR
576 expression rates were quantified by flow cytometry. Cell preparation was adjusted to administer
577 2.5e6 CAR-positive T cells per 100 µL injection. Finally, 100 µL TaSEL was administered on Day
578 0 via tail vein injection.

579 **Peripheral bleeds.** Submandibular blood was collected by puncturing the vein slightly
580 behind the mandible and below the ear canal with a 4mm animal lancet. Blood was collected in
581 heparin tubes and mice were monitored for recovery. In the event a submandibular bleed could
582 not be initiated, blood was collected from the tail vein using a lancet.

583 **IVIS imaging.** Mice were injected with D-luciferin (PerkinElmer, XenoLight) at 150ug/g
584 body weight, prepared following manufacturer's instructions. After a 15 minute incubation, mice
585 were anesthetized with 1% isoflurane. Mice were then transferred to a Perkin Elmer IVIS
586 Spectrum CT and luciferase signals were obtained by bioluminescence imaging. Mice were
587 imaged on average every 3 days during tumor challenge experiments.

588 **Endpoint.** When endpoints were reached in accordance with Body Condition Scoring,
589 mice were sacrificed CO_2 and terminal bleeds. Blood, spleen, liver, and lung samples were
590 collected for analysis. Single-cell suspensions of spleen were prepared by pressing the organ
591 through 70 µm filters with the back of a 1 mL syringe. Splenocytes were isolated by filtering
592 collected blood through a 70 µm filter, followed by lysis of erythrocytes (ACK Lysing Buffer,
593 Gibco). Lung and liver samples were prepared as described in *Multiplex Immunofluorescence*
594 *Staining, Imaging, and Analysis*.

595

596 **Vector design**

597 MoV envelope proteins were purchased as gene blocks from GenScript and expressed
598 from a CMV promoter from plasmid pCG-Hc∆18 (addgene 84817). Lentiviral reporter transfer
599 vectors were generated from pLX311-Cas9 (addgene 118018) with Cas9 swapped with GFP.
600 CAR lentiviral transfer vectors were pSLCAR-CD19-BBx (addgene 135992).

601 Hybridomas were sequenced by GenScript to determine the VH and VL domains. Single
602 chain variable fragments were designed by linking the VH and VL domains with a flexible linker
603 $(G_4S)_3$ then codon optimized for human expression and gene blocks ordered from GenScript.
604 VHH sequences were similarly codon optimized and ordered. MoV-H-scFv/VHH fusions were
605 cloned into the pCG backbone.

606 Sequence for the co-stimulatory αCD3 (OKT3 clone)-P2A-hCD80 (UniProt sequence)
607 were purchased as a gene block from GenScript and Gateway assembled into a lentiviral
608 transgene vector pLEX-307 (addgene 41392) to be stably expressed from an EF1a promoter.
609
610 **Lentiviral Preparations**
611 For LVs retargeted with morbillivirus envelope proteins, LentiX-293T cells were
612 transfected with morbillivirus H and F envelope plasmids, packaging plasmid psPAX2 (Addgene:
613 12260) and transfer plasmid at a 5:3:24:32 ratio, with 2μg plasmids DNA transfected per 1e6 cell
614 seeded. For VSV-G LV, Lenti-X 293T cells were transfected with VSV-G envelope (pMD2.G,
615 Addgene:12259), psPAX2 and transfer plasmid at a ratio of 1:3:4. The media was changed 8
616 hours post transfection. Supernatant collected 48 hours post media change was purified by 0.45
617 um SFCA filter membrane. For in vitro assays, particles were concentrated 100-fold by incubation
618 with Lenti-X™ Concentrator (Takara Cat. #631232) overnight before being spun down at 1500 x
619 g for 45 minutes. For *in vivo* assays, particles were concurrently spun in 30mL increments in an
620 ultracentrifuge at 24,000 rpm for 2hrs. Resulting pellets were supplemented with PBS and left to
621 resuspend overnight at 4°C. Concentrated stocks were aliquoted and stored at -80°C.
622 Optimization of large scale production, concentration, and characterization was guided by
623 previously published protocols [77].
624
625 **Vector Copy Number**
626 Lentiviral preparations were quantified for vector copy number using the Lenti-X™ qRT-
627 PCR Titration Kit (Takara Bio Cat: #631235). In brief, during lentiviral preparation, aliquots were
628 taken directly after viral supernatant was collected and filtered. RNA was isolated from each
629 sample as per the manufacturer's instructions and then frozen. On day of titering, samples were
630 thawed and prepared on ice, on a lab bench thoroughly cleaned with RNaseZap™ RNase
631 Decontamination Wipes (ThermoFisher, AM9788). Samples were diluted and plated as per the
632 Lenti-X™ qRT-PCR Titration Kit instructions and then analyzed by qRT-PCR using a Thermo
633 Fisher QStudio 6 FLX real-Time PCR System.
634 HIV p24 content was quantified using the PerkinElmer HIV p24 AlphaLISA kit (no longer
635 available from PerkinElmer). Briefly, aliquots of unconcentrated and concentrated viral
636 supernatant were diluted and plated per manufacturer's instructions. AlphaLISA acceptor beads
637 and biotinylated anti-HIV p24 antibodies were incubated at room temperature for 1 hour.
638 Streptavidin donor beads were prepared and added to the samples in a dark BL2+ room (<100
639 lumens) and incubated in the dark at room temperature for 30 minutes. Plate was subsequently
640 read on a PerkinElmer Envision Plate Reader and analyzed using the manufacturer's AlphaLISA
641 analysis protocol for GraphPad Prism.
642
643 **Cell culture**
644 LentiX-293T cells were cultured in Dulbecco's modified Eagle's medium (Gibco)
645 supplemented with 10% fetal bovine serum (FBS), Gentamicin, Penicillin and Streptomycin.
646 HEK293T cells were sub-cultured three times a week at ratios of either 1:10 or 1:20. A20s and
647 NALM6 cells were both cultured in RPMI with similar supplementation. These cells were sub-
648 cultured 3 times a week at a ratio of 1:10. Primary human Pan T cells from Stemcell Technology
649 were cultured in RPMI supplemented with 10% FBS along with Gentamicin, Pen-Strep, 1x

650 NEAA(Life Technologies), 10mM HEPES (Thermo Scientific), 1mM Sodium pyruvate, 55uM 2-
651 Mercaptoethanol (Thermo).
652
653 **Serum envelope protein binding assay**
654 LentiX HEK293T cells were transfected as previously described with 1ug of plasmid
655 encoding the target envelope protein. 16 hours later, human serum samples of known MeV IgG
656 titer were thawed and heat inactivated for 20 minutes at 56°C. Following heat inactivation,
657 stepwise 10-fold dilutions were made of the serum samples with pre-warmed DMEM (formulated
658 as previously described). The transfected cells were then lifted and re-plated in serum dilutions in
659 triplicate. Cells were left to incubate on ice for 1 hour. Following incubation, cells were stained
660 with fluorescent antibodies against Human IgG(APC) (Biolegend, clone: M1310G05) and HA-tag
661 (BioLegend, clone: 16B12) using standard indirect flow cytometry staining protocol. Cells were
662 then analyzed by flow cytometry using a Beckman CytoFLEX LX.
663
664 ***In vitro* CAR T cell activation and killing assay**
665 Re-targeted LV was prepared as previously described, in brief: HEK293s, either
666 unmodified or stably expressing co-stimulatory αCD3-hCD80, were transfected with env plasmids
667 encoding VSV-G or MeV/DMV-H-aCD7^{VHH}; DMV/MeV-F^{311} as well as plasmids encoding a anti-
668 CD19-CAR-GFP transgene. Donor Pan T cells were cultured and stimulated with Dynabeads™
669 Human T-Activator CD3/CD28 beads (Gibco™ 11131D) for 24 hours. Dynabeads were then
670 removed from solution via magnets, and Pan T cells were washed following Dynabead
671 manufacturer's instructions. CD19+ NALM6 cells and activated Pan-T cells were then plated in
672 various effector-target ratios and 10uL of 100-fold concentrated re-targeted LV was added to
673 corresponding wells. 3 days and 6 days post-plating, aliquots from each well were taken, stained
674 with aCD19 (Biolegend HIB19) antibody to determine NALM6 populations and analyzed by flow
675 cytometry.
676
677 **Surface expression**
678 For surface expression 1E6 number of HEK293s were seeded and the next day 1ug of
679 envelope plasmid was transfected with BLANK. For HA tagged proteins 24 after transfections
680 cells were stained with anti HA antibody (BioLegend, clone: 16B12) for 1 hour. For surface of
681 untagged MeV-H and MeV-F 10ug/mL of primary mouse anti-MeV-H (CL55) and mouse anti-
682 MeV-F (Y503) were incubated for 2 hours at 4°C followed by a wash with cold MACS buffers then
683 incubated with anti-mouse IgG (Biolegend, clone: Poly4053) antibody for 1 hour.
684
685 **Serum Neutralization Assay**
686 Serum donor samples were received from the Mass General Brigham BioBank and stored
687 at -80°C. Samples were quantified for human IgG against MeV using a MeV IgG ELISA kit
688 (Abcam: ab108750). Seropositivity was determined using a cut-off control well following the
689 manufacturer's instructions.
690 Re-targeted LV was prepared as previously described, in brief: unmodified HEK293T
691 producer cells were transfected with env plasmids encoding different env protein variants as well
692 as a transgene plasmid encoding aCD19-CAR-GFP. Supernatant was collected as previously
693 described. Human serum samples of known MeV IgG titer were thawed and heat inactivated for

694 20 minutes at 56°C. Following heat inactivation, stepwise 10-fold dilutions were made of the
695 serum samples with pre-warmed DMEM (formulated as previously described) in a 96well plate.
696 Retargeted LV was then plated into the serum dilutions and left to incubate on ice for 1 hour.
697 Following incubation, A20 lymphoma cells were plated in the wells. 48 hours later aliquots of each
698 well were collected and analyzed by flow cytometry. "Remaining transduction" was calculated by
699 dividing the %GFP+ cells for a well of a given LV and serum dilution by the %GFP+ cells for that
700 LV in the control well containing no serum.
701
702 **Multiplex Immunofluorescence Staining, Imaging, and Analysis**
703 After mice were sacrificed, tissues were harvested and fixed in neutral buffered formalin
704 for 20 hours. Tissus were then embedded in paraffin, and sectioned at 4-5 µm. Tissues were
705 deparaffinized and hydrated by baking at 65°C for 15 minutes followed by a xylene and an ethanol
706 gradient. Antigen retrieval was performed with a citrate-based buffer (Vector Labs) for 45 minutes
707 at 100°C. Following antigen retrieval, cyclic immunofluorescence staining and imaging was
708 performed using a Lunaphore Comet with primary antibodies targeting human CD3 (CD3-12,
709 Abcam) mouse F4/80 (D2S9R, Cell Signalling), mouse Arginase-1(D4E3M, Cell Signaling), and
710 GFP (600-101-215, Rockland). Secondary staining was performed with Donkey Anti-Rabbit IgG
711 AlexaFluor 647+, Donkey Anti-Rabbit IgG AlexaFluor 555+, or Donkey anti-Goat IgG AlexaFluor
712 647+ (Life Technologies). Background subtraction was performed with Horizon Viewer
713 (Lunaphore). Corrected images were then analyzed using Qupath[78].
714 Areas of tissue folding or large tissue artifacts were excluded from analysis. On analyzable
715 tissue, cell segmentation was performed using Instaseg utilizing signal outputs from all fluorescent
716 parameters except for GFP[79]. Cell classifiers were then trained to classify segmented cells based
717 upon their staining for DAPI, CD3, F4/80, and Arginase-1 (CD3+,F4/80-, Arginase-1-;
718 CD3+,F4/80+, Arginase-1-; CD3-,F4/80+,Arginase-1-; CD3-,F4/80-,Arginase-1+; CD3-, F4/80-
719 ,Arginase-1-, Debris/RBCs, Annuclear cells) with an average of 130 annotation per sample.
720 Annotations were made blinded to GFP signal. A Random trees classifier was utilized with
721 consideration of all available fluorescent and geometric parameters except for those directly
722 related to GFP signal. Model classification was manually reviewed to ensure accuracy.
723 GFP-positivity was defined using a threshold of up to 3.5 standard deviations above the
724 mean background fluorescence of the analyzed area of the image (as this would yield < 5 false
725 positive cells per 150,000 cell section due to background alone). Following thresholding, manual
726 review was of all cells in all categories above the threshold. Mis-classified cells were reclassified
727 appropriately. Cells with GFP staining that were wholly discordant with cellular staining or not
728 associated with true cells were excluded as staining/imaging artifacts. CD3+, F4/80+, Arginase-
729 1- cells (likely representing macrophage-lymphocyte pairs or phagocytosed T cells) were
730 excluded from this analysis. Annotations with cell area <12 µm2 were excluded from final analysis
731 as these were primarily cell fragments and debris.

732 ## References

733 1. Merten, O.-W., Hebben, M. & Bovolenta, C. Production of lentiviral vectors. *Mol Ther*
734 *Methods Clin Dev* **3**, 16017 (2016).
735 2. Raguram, A., Banskota, S. & Liu, D. R. Therapeutic in vivo delivery of gene editing agents.
736 *Cell* **185**, 2806–2827 (2022).
737 3. Milone, M. C. & O'Doherty, U. Clinical use of lentiviral vectors. *Leukemia* **32**, 1529–1541
738 (2018).
739 4. Sweeney, N. P. & Vink, C. A. The impact of lentiviral vector genome size and producer cell
740 genomic to gag-pol mRNA ratios on packaging efficiency and titre. *Mol Ther Methods Clin*
741 *Dev* **21**, 574–584 (2021).
742 5. Abordo-Adesida, E. *et al.* Stability of lentiviral vector-mediated transgene expression in the
743 brain in the presence of systemic antivector immune responses. *Hum. Gene Ther.* **16**, 741–
744 751 (2005).
745 6. Baekelandt, V., Eggermont, K., Michiels, M., Nuttin, B. & Debyser, Z. Optimized lentiviral
746 vector production and purification procedure prevents immune response after transduction
747 of mouse brain. *Gene Ther.* **10**, 1933–1940 (2003).
748 7. Argaw, T. *et al.* In vivo targeting of lentiviral vectors pseudotyped with the Tupaia
749 paramyxovirus H glycoprotein bearing a cell-specific ligand. *Mol Ther Methods Clin Dev* **21**,
750 670–680 (2021).
751 8. Frank, A. M. & Buchholz, C. J. Surface-Engineered Lentiviral Vectors for Selective Gene
752 Transfer into Subtypes of Lymphocytes. *Mol Ther Methods Clin Dev* **12**, 19–31 (2019).
753 9. Buchholz, C. J., Friedel, T. & Büning, H. Surface-Engineered Viral Vectors for Selective and
754 Cell Type-Specific Gene Delivery. *Trends Biotechnol.* **33**, 777–790 (2015).
755 10. Zhou, Q. *et al.* T-cell receptor gene transfer exclusively to human CD8(+) cells enhances
756 tumor cell killing. *Blood* **120**, 4334–4342 (2012).

757 11. Zhou, Q. *et al.* Exclusive Transduction of Human CD4+ T Cells upon Systemic Delivery of
758 CD4-Targeted Lentiviral Vectors. *J. Immunol.* **195**, 2493–2501 (2015).
759 12. Verhoeyen, E. *et al.* IL-7 surface-engineered lentiviral vectors promote survival and efficient
760 gene transfer in resting primary T lymphocytes. *Blood* **101**, 2167–2174 (2003).
761 13. Maurice, M. *et al.* Efficient gene transfer into human primary blood lymphocytes by surface-
762 engineered lentiviral vectors that display a T cell-activating polypeptide. *Blood* **99**, 2342–
763 2350 (2002).
764 14. Yang, L., Bailey, L., Baltimore, D. & Wang, P. Targeting lentiviral vectors to specific cell
765 types in vivo. *Proc. Natl. Acad. Sci. U. S. A.* **103**, 11479–11484 (2006).
766 15. Funke, S. *et al.* Pseudotyping lentiviral vectors with the wild-type measles virus
767 glycoproteins improves titer and selectivity. *Gene Ther.* **16**, 700–705 (2009).
768 16. Lévy, C. *et al.* Measles virus envelope pseudotyped lentiviral vectors transduce quiescent
769 human HSCs at an efficiency without precedent. *Blood Adv* **1**, 2088–2104 (2017).
770 17. Anliker, B. *et al.* Specific gene transfer to neurons, endothelial cells and hematopoietic
771 progenitors with lentiviral vectors. *Nat. Methods* **7**, 929–935 (2010).
772 18. Hashiguchi, T. *et al.* Structure of the measles virus hemagglutinin bound to its cellular
773 receptor SLAM. *Nat. Struct. Mol. Biol.* **18**, 135–141 (2011).
774 19. Navaratnarajah, C. K., Leonard, V. H. J. & Cattaneo, R. Measles virus glycoprotein
775 complex assembly, receptor attachment, and cell entry. *Curr Top Microbiol Immunol* **329**,
776 59–76 (2009).
777 20. White, J. M., Delos, S. E., Brecher, M. & Schornberg, K. Structures and mechanisms of
778 viral membrane fusion proteins: multiple variations on a common theme. *Crit. Rev.*
779 *Biochem. Mol. Biol.* **43**, 189–219 (2008).
780 21. Duvergé, A. & Negroni, M. Pseudotyping Lentiviral Vectors: When the Clothes Make the
781 Virus. *Viruses* **12**, (2020).
782 22. Ou, W. *et al.* Specific targeting of human interleukin (IL)-13 receptor α2-positive cells with

783 lentiviral vectors displaying IL-13. *Hum. Gene Ther. Methods* **23**, 137–147 (2012).
784 23. Frank, A. M. *et al.* CD8-Specific Designed Ankyrin Repeat Proteins Improve Selective Gene
785 Delivery into Human and Primate T Lymphocytes. *Hum. Gene Ther.* **31**, 679–691 (2020).
786 24. Münch, R. C. *et al.* DARPins: an efficient targeting domain for lentiviral vectors. *Mol. Ther.*
787 **19**, 686–693 (2011).
788 25. Friedel, T. *et al.* Receptor-targeted lentiviral vectors are exceptionally sensitive toward the
789 biophysical properties of the displayed single-chain Fv. *Protein Eng. Des. Sel.* **28**, 93–106
790 (2015).
791 26. Lech, P. J. *et al.* Antibody neutralization of retargeted measles viruses. *Virology* **454-455**,
792 237–246 (2014).
793 27. Bah, E. S., Nace, R. A., Peng, K. W., Muñoz-Alía, M. Á. & Russell, S. J. Retargeted and
794 Stealth-Modified Oncolytic Measles Viruses for Systemic Cancer Therapy in Measles
795 Immune Patients. *Mol Cancer Ther* **19**, 2057–2067 (2020).
796 28. Marino, M. P. *et al.* A scalable method to concentrate lentiviral vectors pseudotyped with
797 measles virus glycoproteins. *Gene Ther.* **22**, 280–285 (2015).
798 29. Chiu, M. L., Goulet, D. R., Teplyakov, A. & Gilliland, G. L. Antibody structure and function:
799 The basis for engineering therapeutics. *Antibodies (Basel)* **8**, 55 (2019).
800 30. Sun, W. *et al.* A combined strategy improves the solubility of aggregation-prone single-
801 chain variable fragment antibodies. *Protein Expr. Purif.* **83**, 21–29 (2012).
802 31. Ahmad, Z. A. *et al.* scFv antibody: principles and clinical application. *Clin. Dev. Immunol.*
803 **2012**, 980250 (2012).
804 32. Strebinger, D. *et al.* Cell type-specific delivery by modular envelope design. *Nat. Commun.*
805 **14**, 5141 (2023).
806 33. Dobson, C. S. *et al.* Antigen identification and high-throughput interaction mapping by
807 reprogramming viral entry. *Nat. Methods* **19**, 449–460 (2022).
808 34. Hamilton, J. R. *et al.* In vivo human T cell engineering with enveloped delivery vehicles.

809 *Nat. Biotechnol.* (2024) doi:10.1038/s41587-023-02085-z.
810 35. Nikolic, J. *et al.* Structural basis for the recognition of LDL-receptor family members by VSV
811 glycoprotein. *Nat Commun* **9**, 1029 (2018).
812 36. Sun, X., Yau, V. K., Briggs, B. J. & Whittaker, G. R. Role of clathrin-mediated endocytosis
813 during vesicular stomatitis virus entry into host cells. *Virology* **338**, 53–60 (2005).
814 37. Morizono, K. *et al.* The soluble serum protein Gas6 bridges virion envelope
815 phosphatidylserine to the TAM receptor tyrosine kinase Axl to mediate viral entry. *Cell Host*
816 *Microbe* **9**, 286–298 (2011).
817 38. Sommermeyer, D. *et al.* Chimeric antigen receptor-modified T cells derived from defined
818 CD8+ and CD4+ subsets confer superior antitumor reactivity in vivo. *Leukemia* **30**, 492–
819 500 (2016).
820 39. Russell, S. J. *et al.* Remission of disseminated cancer after systemic oncolytic virotherapy.
821 *Mayo Clin. Proc.* **89**, 926–933 (2014).
822 40. Dispenzieri, A. *et al.* Phase I trial of systemic administration of Edmonston strain of measles
823 virus genetically engineered to express the sodium iodide symporter in patients with
824 recurrent or refractory multiple myeloma. *Leukemia* **31**, 2791–2798 (2017).
825 41. Lévy, C. *et al.* Lentiviral vectors displaying modified measles virus gp overcome pre-
826 existing immunity in in vivo-like transduction of human T and B cells. *Mol Ther* **20**, 1699–
827 1712 (2012).
828 42. Abramson, J. *et al.* Accurate structure prediction of biomolecular interactions with
829 AlphaFold 3. *Nature* **630**, 493–500 (2024).
830 43. Bouche, F. B., Ertl, O. T. & Muller, C. P. Neutralizing B cell response in measles. *Viral*
831 *Immunol.* **15**, 451–471 (2002).
832 44. de Swart, R. L., Yüksel, S., Langerijs, C. N., Muller, C. P. & Osterhaus, A. D. M. E.
833 Depletion of measles virus glycoprotein-specific antibodies from human sera reveals
834 genotype-specific neutralizing antibodies. *J. Gen. Virol.* **90**, 2982–2989 (2009).

835 45. de Swart, R. L., Yüksel, S. & Osterhaus, A. D. M. E. Relative contributions of measles virus
836 hemagglutinin- and fusion protein-specific serum antibodies to virus neutralization. *J. Virol.*
837 **79**, 11547–11551 (2005).
838 46. Bender, R. R. *et al.* Receptor-Targeted Nipah Virus Glycoproteins Improve Cell-Type
839 Selective Gene Delivery and Reveal a Preference for Membrane-Proximal Cell Attachment.
840 *PLoS Pathog.* **12**, e1005641 (2016).
841 47. Plattet, P. *et al.* Conserved leucine residue in the head region of morbillivirus fusion protein
842 regulates the large conformational change during fusion activity. *Biochemistry* **48**, 9112–
843 9121 (2009).
844 48. von Messling, V. & Cattaneo, R. Amino-terminal precursor sequence modulates canine
845 distemper virus fusion protein function. *J. Virol.* **76**, 4172–4180 (2002).
846 49. von Messling, V., Milosevic, D., Devaux, P. & Cattaneo, R. Canine distemper virus and
847 measles virus fusion glycoprotein trimers: partial membrane-proximal ectodomain cleavage
848 enhances function. *J. Virol.* **78**, 7894–7903 (2004).
849 50. Funke, S. *et al.* Targeted cell entry of lentiviral vectors. *Mol. Ther.* **16**, 1427–1436 (2008).
850 51. Muñoz-Alía, M. A. & Russell, S. J. Probing Morbillivirus Antisera Neutralization Using
851 Functional Chimerism between Measles Virus and Canine Distemper Virus Envelope
852 Glycoproteins. *Viruses* **11**, (2019).
853 52. Corey Elizabeth A. & Iorio Ronald M. Mutations in the Stalk of the Measles Virus
854 Hemagglutinin Protein Decrease Fusion but Do Not Interfere with Virus-Specific Interaction
855 with the Homologous Fusion Protein. *J. Virol.* **81**, 9900–9910 (2007).
856 53. Rust, B. J. *et al.* Envelope-Specific Adaptive Immunity following Transplantation of
857 Hematopoietic Stem Cells Modified with VSV-G Lentivirus. *Mol Ther Methods Clin Dev* **19**,
858 438–446 (2020).
859 54. DePolo, N. J. *et al.* VSV-G pseudotyped lentiviral vector particles produced in human cells
860 are inactivated by human serum. *Mol Ther* **2**, 218–222 (2000).

861 55. Baldauf, H.-M. *et al.* SAMHD1 restricts HIV-1 infection in resting CD4(+) T cells. *Nat. Med.*
862 **18**, 1682–1687 (2012).
863 56. Doitsh, G. *et al.* Abortive HIV infection mediates CD4 T cell depletion and inflammation in
864 human lymphoid tissue. *Cell* **143**, 789–801 (2010).
865 57. Zack, J. A. *et al.* HIV-1 entry into quiescent primary lymphocytes: molecular analysis
866 reveals a labile, latent viral structure. *Cell* **61**, 213–222 (1990).
867 58. Finkelshtein, D., Werman, A., Novick, D., Barak, S. & Rubinstein, M. LDL receptor and its
868 family members serve as the cellular receptors for vesicular stomatitis virus. *Proc. Natl.*
869 *Acad. Sci. U. S. A.* **110**, 7306–7311 (2013).
870 59. Amirache, F. *et al.* Mystery solved: VSV-G-LVs do not allow efficient gene transfer into
871 unstimulated T cells, B cells, and HSCs because they lack the LDL receptor. *Blood* **123**,
872 1422–1424 (2014).
873 60. Zhang, D. K. Y. *et al.* Enhancing CAR-T cell functionality in a patient-specific manner. *Nat.*
874 *Commun.* **14**, 1–13 (2023).
875 61. Mescher, M. F. *et al.* Signals required for programming effector and memory development
876 by CD8+ T cells. *Immunol. Rev.* **211**, 81–92 (2006).
877 62. Melenhorst, J. J. *et al.* Decade-long leukaemia remissions with persistence of CD4+ CAR T
878 cells. *Nature* **602**, 503–509 (2022).
879 63. van Til, N. P. *et al.* Kupffer cells and not liver sinusoidal endothelial cells prevent lentiviral
880 transduction of hepatocytes. *Mol. Ther.* **11**, 26–34 (2005).
881 64. Milani, M. *et al.* Phagocytosis-shielded lentiviral vectors improve liver gene therapy in
882 nonhuman primates. *Sci. Transl. Med.* **11**, (2019).
883 65. Morizono, K. *et al.* Redirecting lentiviral vectors pseudotyped with Sindbis virus-derived
884 envelope proteins to DC-SIGN by modification of N-linked glycans of envelope proteins. *J*
885 *Virol* **84**, 6923–6934 (2010).
886 66. Ziegler, L. *et al.* Targeting lentiviral vectors to antigen-specific immunoglobulins. *Hum.*

887 *Gene Ther.* **19**, 861–872 (2008).
888 67. Zhang, X.-Y. *et al.* Cell-specific targeting of lentiviral vectors mediated by fusion proteins
889 derived from Sindbis virus, vesicular stomatitis virus, or avian sarcoma/leukosis virus.
890 *Retrovirology* **7**, 3 (2010).
891 68. Aires da Silva, F., Costa, M. J. L., Corte-Real, S. & Goncalves, J. Cell type-specific
892 targeting with sindbis pseudotyped lentiviral vectors displaying anti-CCR5 single-chain
893 antibodies. *Hum. Gene Ther.* **16**, 223–234 (2005).
894 69. Muñoz-Alía, M. Á., Nace, R. A., Zhang, L. & Russell, S. J. Serotypic evolution of measles
895 virus is constrained by multiple co-dominant B cell epitopes on its surface glycoproteins.
896 *Cell Rep. Med.* **2**, 100225 (2021).
897 70. Aditi & Shariff, M. Nipah virus infection: A review. *Epidemiol. Infect.* **147**, e95 (2019).
898 71. Pallister, J. A. *et al.* Vaccination of ferrets with a recombinant G glycoprotein subunit
899 vaccine provides protection against Nipah virus disease for over 12 months. *Virol. J.* **10**,
900 237 (2013).
901 72. Nieba, L., Honegger, A., Krebber, C. & Plückthun, A. Disrupting the hydrophobic patches at
902 the antibody variable/constant domain interface: improved in vivo folding and physical
903 characterization of an engineered scFv fragment. *Protein Eng.* **10**, 435–444 (1997).
904 73. Xu, J. *et al.* Nanobodies from camelid mice and llamas neutralize SARS-CoV-2 variants.
905 *Nature* **595**, 278–282 (2021).
906 74. Ruffin, N. *et al.* Low SAMHD1 expression following T-cell activation and proliferation
907 renders CD4+ T cells susceptible to HIV-1. *AIDS* **29**, 519–530 (2015).
908 75. Uchida, N. *et al.* TRIM5α variation affects Lentiviral transduction efficiency for long-term
909 hematopoietic repopulating cells in a rhesus stem cell transplantation model. *Blood* **118**,
910 2056–2056 (2011).
911 76. Arcangeli, S. *et al.* CAR T cell manufacturing from naive/stem memory T lymphocytes
912 enhances antitumor responses while curtailing cytokine release syndrome. *J. Clin. Invest.*

913 **132**, (2022).

914 77. Weidner, T. *et al.* Genetic in vivo engineering of human T lymphocytes in mouse models.

915 *Nature Protocols* **16**, 3210–3240 (2021).

916 78. Bankhead, P. *et al.* QuPath: Open source software for digital pathology image analysis.

917 *Scientific Reports* **7**, 1–7 (2017).

918 79. Goldsborough, T. *et al.* A novel channel invariant architecture for the segmentation of cells

919 and nuclei in multiplexed images using InstanSeg. *Bioinformatics* (2024).